MAMBA

GO FLY

SPONSORED BY BOEING

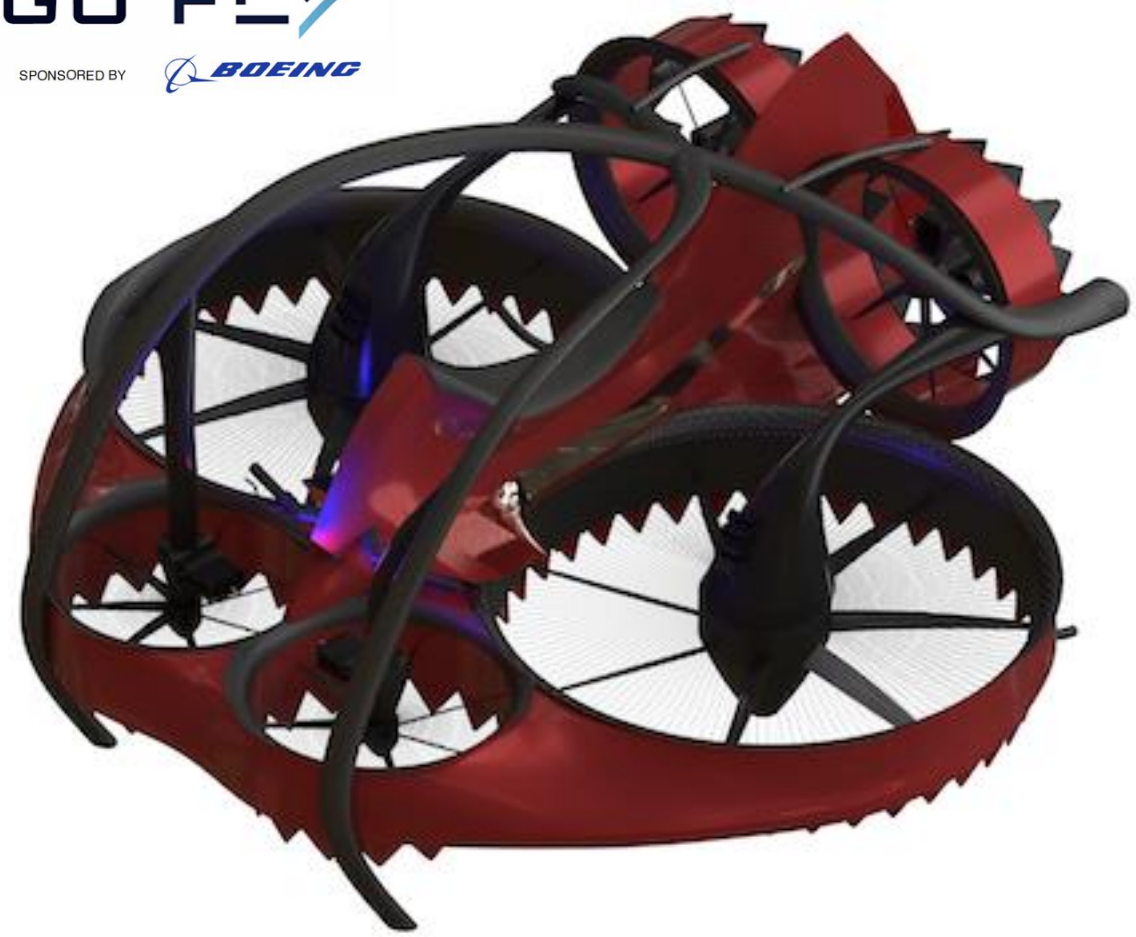

Vertical Takeoff and Landing Personal Flying Machine

The University of Kansas

Lauren Schumacher (Team Leader), John Haug, Martin Mendoza, Patrick McNamee, Joshua Mudd, Ankur Patil, Dalton Prins, Nicholas Werner

Prof. Ronald Barrett-Gonzalez (Advisor)

June 2018

TABLE OF CONTENTS

LIST OF FIGURES

LIST OF TABLES

List of Symbols and Acronyms

A	Area	ft^2
AEO	All Engines Operating	(-)
ASL	Above Sea Level	(ft)
BEMT	Blade Element Momentum Theory	(-)
C_{d0}	Section Zero-Lift Drag Coefficient	(-)
CG	Center of Gravity	in
C_L	Coefficient of Lift	(-)
C_p	Power Coefficient	(-)
D	Drag	lbf
DL	Disk Loading	lbf/ft^2
E	Endurance	hr
e	Oswald's Efficiency Factor	(-)
f	Parasite Area	ft^2
FEM	Finite Element Model	(-)
FM	Figure of Merit	(-)
IC	Internal Combustion	(-)
J	Mass Moment of Inertia	$lb_m ft^2$
L	Lift	lbf
L	Aerodynamic Moment Component about x	lbf-ft
M	Aerodynamic Moment Component about y	lb-ft
m_{ff}	Mass Fuel Fraction	(-)
MGTOW	Max Gross Takeoff Weight	lbf
MSL	Mean Sea Level	(ft)
N	Number of Engines	(-)
N	Aerodynamic Moment Component about z	lbf-ft
n	Number of G's	(g)
P	Angular Velocity Component about x	rad/s
q	Dynamic Pressure	lbf/ft2
Q	Angular Velocity Component about y	rad/s
R	Range	(ft)
R	Angular Velocity Component about z	rad/s
r_D	Mean Drag Radius	ft
S	Surface Area	ft^2
SFC	Specific Fuel Consumption	lb_f-hp/hr
SPL	Sound Pressure Level	dB
S_{WET}	Wetted Area	ft^2
T	Thrust	lbf
TRL	Technology Readiness Level	(-)
U	Velocity Component along x	ft/s
V	True Air Speed	kts, ft/s
V	Velocity Component along y	ft/s

V_i	Induced Velocity	ft/s
W	Weight	lbf
W	Velocity Component along z	ft/s
κ	Induced Power Factor	(-)
λ	Rotor Inflow Ratio	(-)
μ	Advance Ratio	(-)
θ	Optimization Weighting Factor	(-)
θ	Blade Pitch Angle	rad., deg.
ρ	Density	slug/ft^3
σ	Solidity	(-)
ϕ	Inflow Angle of Attack	rad., deg.
ψ	Azimuth Angle	rad., deg.

MAMBA DESIGN FEATURES

I. **Safe Flight Design**
- FAR 21 compliant, 10^{-6} failure probability design
- OEI climb-out, 900 ft/min at 5,000 ft ISA (FAR 29.67 compatible)
- Integral wire-splitter, roll cage, and ballistic chute mount
- Min. flight risk → low insurance premium, high customer acceptance

II. **Exceeds All Performance Objectives**
- 7.9' max linear dim. ($\theta_{Size} = 0.58$)
- 67dBA @ 50' ($\theta_{Noise} = 5.08$)
- Max speed 60 kts ($\theta_{Speed} = 0.68$)

III. **MicroStator Acoustic Suppression System**
- Patent pending, experimentally proven
- >3dBA SPL reduction WRT state-of-the-art ducted fans

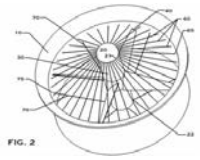

Figure 1: US Patent Pending (62/659,026)

Advanced Flight Control System:
- Triple Redundancy
- Intuitive Controls for Inexperienced Pilots
- FAA Compliant Geofencing

Attention to Safety:
- 10^{-6} Failure Mode Design
- FAR-21 Compliant
- Compatible with FAR-29.67 OEI (via cross-shafting)
- Tight MicroStator meshing mitigates FOD & injury

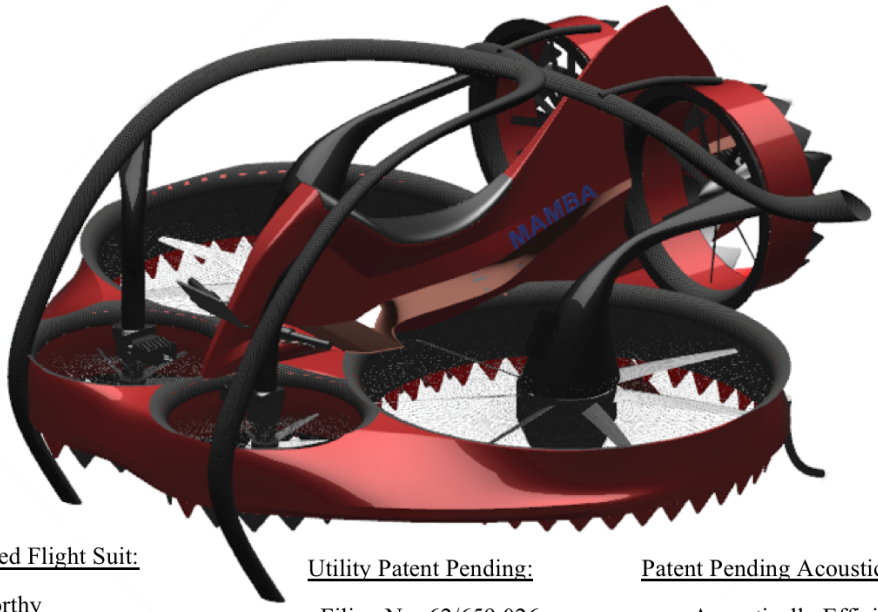

Advanced Flight Suit:
- Crashworthy
- Aerodynamically Efficient
- Ergonomic

Utility Patent Pending:
- Filing No. 62/659,026
- Ultra-quiet, Safe, and Certifiable Duct Technology

Patent Pending Acoustic MicroStators:
- Acoustically Efficient
- Lightweight
- Pre-Swirl/De-swirl Thrust Enhancement
- Vibration Resistant/Quiet

1. INTRODUCTION

1.1 MISSION SPECIFICATION AND DERIVED OPERATING CONDITIONS

The goal of the GoFly competition is to create a personal VTOL experience as a technology demonstrator to jumpstart the industry. The mission specification provided by the competition led to derived operating conditions simplified in Figure 2. These conditions were used to size the airframe and systems outlined in this document.

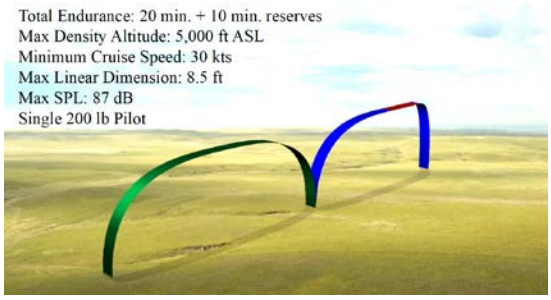

Figure 2: Mission Specification (10)

1.2 HISTORICAL ANALYSIS

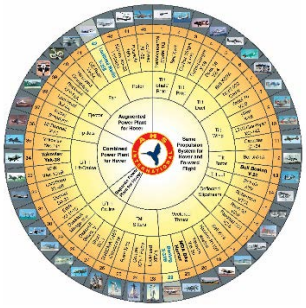

Figure 3: V/STOL Configurations

Many attempts at creating a viable VTOL vehicle have been attempted. Historically, the designs may be summarized as part of the fabled V/STOL configuration wheel (Figure 3). Some of the historically significant designs are outlined in this section to show the diversity in the personal VTOL concept.

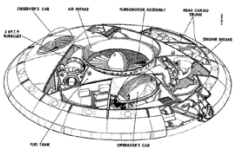

The Avro Canada VZ-9 program was initiated in 1952 as a high speed VTOL craft. The aircraft is reminiscent of "flying saucers," but was designed to take advantage of the Coandă Effect to provide enhanced lift and thrust in operation. The concept was scrapped when instabilities were encountered at elevations above 3 ft (1).

The 1955 Hiller VZ-1 VTOL design used a single ducted fan to provide lift and thrust. Control was accomplished via kinesthetic control by the pilot leaning to shift the aircraft CG. The design suffered from instabilities, though it proved to be a great technology demonstrator for early VTOL and ducted fan concepts. Military utilization was hampered by low top speed and mission design (2).

Glenn Martin began research on high endurance personal jetpacks in 1981which continued until 2008 when the Martin Jetpack was introduced at the Oshkosh airshow. The jetpack uses a two-stroke V-4 engine along with ducted fans to generate thrust. The design can carry more than 100 kg for 30 mins; with a range of approximately 20 km and a flight ceiling of 2500 ft. The jetpack is for specialized use, though Martin Company is hoping to have it available for /recreation by 2020, and for personal use by 2030 (3).

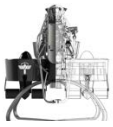

Moller International was founded in 1983 to design, develop, manufacture, and market personal vertical takeoff and landing vehicles. The company has since compiled a family of VTOL concepts; most notably the Skycar 200 autonomous air taxi vehicle, the Skycar 400 tilted duct variant and the Neuera 200 (4). The Neuera resembles the VZ-9 and is marketed as a personal or light utility craft.

2 DESIGN DOWNSELECTION

2.1 CONFIGURATION PARAMETERS

The RFP, heavily weights size and noise and requires optimization in this design. Although not scored in the GoFly competition, emphasis is placed on design safety. Survivability in engine out and crash scenarios is the primary driver in the structural layout of the vehicle. Primary systems are designed to 1 in 10^{-6} failure probability following consultation with FAA office directors and aviation insurance industry executives. Marketability was also deemed critical and consultations with Dr. Lance Rake, a leader in stylistic design, improved the overall final configuration aesthetics. Consultations with individuals from an internationally renowned aviation insurance provider also emphasized both operator and bystander safety, and several key aspects of the design were marked as favorable and are discussed in subsequent sections.

Table 1: Weighting Factors

Design Variable	Weight (%)
Aircraft Size	17.5
Aircraft Noise	22.5
Aircraft Speed	10
Actual Range with Loiter	12
Pilot Sightlines	5
Cost	8
Aircraft Safety	20
Aesthetic Appeal	5

The design configurations used in the down selection process are shown in Figure 11. The preliminary sizing optimization function incorporated the quantitative characteristics obtained with first order methods.

$$S = 0.40\theta_D + .45\theta_{SPL} + .15\theta_{performance} \quad \text{(Eq. 1)}$$

Weighting factors shown in Eq. 1 were used as the configuration deselection criteria. For initial analysis, the performance metric is quantified with the MGTOW of a given configuration normalized to the maximum of the configurations analyzed.

2.2 CONFIGURATION FLY-OFF

Each of the configuration concepts were analyzed using the optimization function provided with a summary provided for the most competitive designs.

Figure 4: Conventional High Rotor

The conventional configuration consisted of a main rotor for lift and a tail rotor for stability and control. This configuration was deemed unfavorable due to size and noise constraints, inadequate tail rotor moment arm on the tail rotor and decreased main rotor efficiency. Safety also precludes the use of a conventional configuration due to the presence of unshielded rotors at less than head height for the provided size constraints.

Figure 5: Conventional Low Rotor

A coaxial contra-rotating configuration consists of two main rotors and is efficient in a constrained design volume. The contra-rotating design configuration was deemed unfavorable for high volumes of generated rotor noise and similar safety concerns to the conventional.

Iterations of multi-copter configurations were also considered. While these designs offer increased safety in terms of single point engine

Figure 7: Coaxial Main Rotor

Figure 6: Ducted Multicopter

and rotor failures, design volume constraints impact overall efficiency. An initial safety review with FAA consultants on open rotor concepts like the Scorpion raised concerns for pilot and bystander safety in both crash scenarios and in standard operating conditions Shrouded rotors allow for a slight increase in thrust efficiencies while enabling support structures to ensure during operation no loss of limb is possible. Additionally the total lifting area may be maximized by displacing the pilot from the rotor plane. The shrouded multi-copter with a vertically displaced pilot concept was selected for a detailed tradeoff study, discussed in later sections, on the number and type of engines.

3 PRELIMINARY SIZING

3.1 WEIGHTS DETERMINATION

The preliminary analysis using techniques from Leishman (5) considered the basic equations for required non-dimensionalized power (Eq. 2) using the most conservative operating condition: hover at 5,000 ft ASL for 30 min.

$$C_P = \frac{\kappa C_T^2}{2\sqrt{\lambda^2+\mu^2}} + \frac{\sigma C_{d0}}{8}(1+K\mu^2) + \frac{1}{2}\left(\frac{f}{A}\right)\mu^2 + \lambda_c C_W \qquad \text{(Eq. 2)}$$

Preliminary MGTOW may be calculated with the known power requirements, including a 25% thrust margin for controllability, for each configuration analyzed by defining engine size.

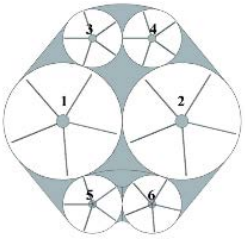

Figure 8: Propulsion Numbering Scheme

3.1.1 PROPULSION ARRANGEMENT

In addition to overall power requirements, preliminary weights sizing also necessitate the selection of a propulsion system type. This type (internal combustion or electric) was defined as an independent variable in the configuration sweep. Powerplant numbering for a notional hexcopter is shown in Figure 8.

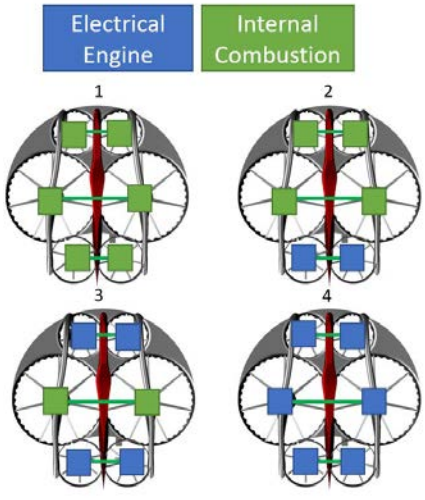

Figure 9: Powerplant Configurations

Four combinations of powerplant types were analyzed (Figure 9). The four layouts investigated include:

1. All internal combustion engines;
2. Two electric motors (5 & 6) and four internal combustion engines (1-4);
3. Four electric motors (3-6) and two internal combustion engine (1 &2);
4. All electric motors.

Each comparison was sized for varying max vehicle diameter. Weights determined for the internal combustion (IC) systems include the engine, electric starter, fuel, and cross shafting components. The electric propulsion includes the motor weight in addition to the batteries required for the max power condition (hover at 5,000 ft

ASL). The battery weight is sized from a nominal energy density and tabulated total power required for the endurance hover. Although battery weight constrains the number of electric propulsion systems onboard the vehicle, plausible MGTOW values for a mixed propulsion system (see Configuration 2) would allow for a decrement in the overall SPL.

3.1.2 Preliminary Weights Summary

With the above propulsion configurations, a detailed study of size, powerplant type, and emergency landing recovery system was made with MGTOW as a performance metric in each of these scenarios, sweeping from 5 to 8.5 ft in maximum dimension. Both ballistic recovery chutes and oversized/cross-shafted engines were studied as feasible means of returning the vehicle safely

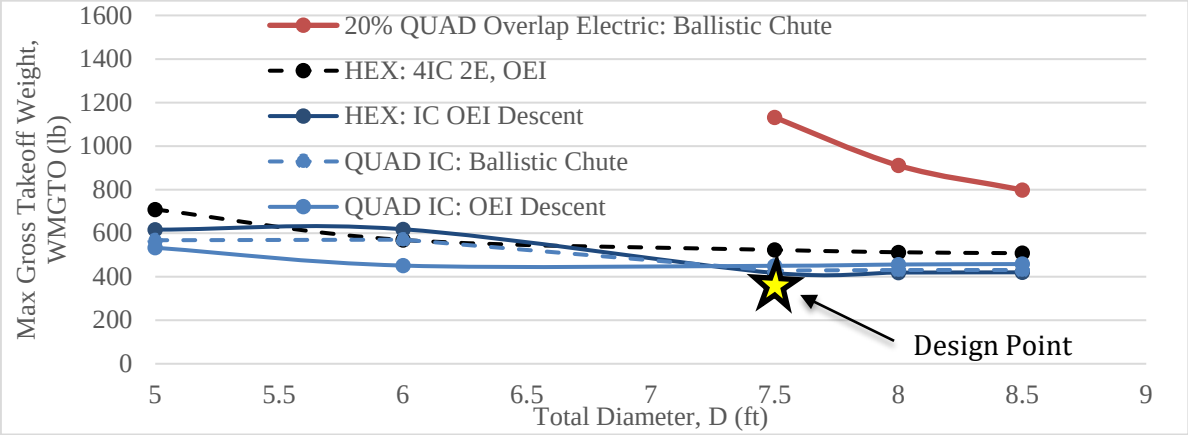

Figure 10: Detailed Multicopter Configuration Study

to the ground in case of engine failure. Both quadcopter and hexcopter arrangements are detailed with the Scorpion 3 notionally sized for comparison.

From Figure 10, it is apparent the larger hexcopter and quadcopter configurations result in deceased MGTOW if the system is of mixed or fully IC type. As there is little variance between the weights of the quad and hex concepts, the hexcopter was selected for final configuration design as it provides the greatest control authority in an engine out scenario. From this study, it is also apparent that a fully IC propulsion system yields the minimum MGTOW. In the following configuration iterations, design features such as shrouded rotors are incorporated to address operator and bystander safety per the concerns noted in the FAA reviews.

3.1.3 Hexcopter Control Scheme

Two methods of control were studied for the hexcopter configuration: a fixed duct hexcopter and tilting duct hexcopter configuration (Figure 11). The first would use a series of louvers below the fore and aft engines for thrust vectoring, while the second would tilt the aft shroud assembly.

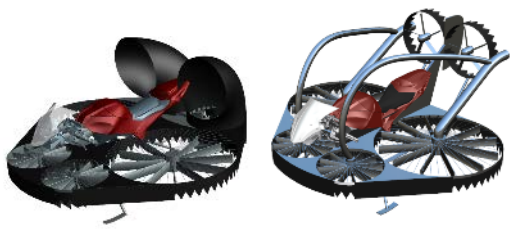

Figure 11: Hexcopter Ducted and Tilted Fan Flightsafe Configurations

Noise is primarily generated by the engine, flow wake-shearing, and rotor interactions. The authors compared the acoustic suppression techniques that could be provided to each configuration. The tilting duct scheme takes advantage of increased design volume for engine

mufflers (and hence engine noise suppression). The fixed duct concept provides additional structure that can hold more broadband acoustic suppression layers, but additional noise is generated with louvers underneath the four auxiliary engines (engines 3-6). Both configurations may take advantage of jet noise suppression techniques such as chevrons. The tilted duct configuration however, will allow for a greater forward flight speed without losses associated from flow turning. The tilting duct configuration was thus selected for further analysis.

4 DETAILED CONFIGURATION REFINEMENT

4.1 WEIGHTS AND POWERPLANT SIZING

4.1.1 WEIGHTS DETERMINATION

The airframe weight was determined with first order structural analysis specifying materials and thicknesses. The airframe weight fractions for the 7.5ft diameter are displayed in Table 3. The powerplants for the vehicle were internal combustion engines, electric starter motors, and the necessary batteries. The internal combustion engines used are a combination of the Freedom Motors Rotapower Engine and the 3W Modellmotoren series. The 7.5 ft diameter configuration utilizes the 30hp Rotapower engines for engines 1&2; each weigh 35lb_f and have a rated S.F.C of 0.45lb/hp-hr. Engines 3&4 use the 10.5hp 3W-85Xi TS CS, weighing 3.5lb_f. The electric starter motors are sized based on the Turnigy Rotamax Brushless motor series. Table 4 demonstrates the final weights of the 7.5 ft diameter vehicle for the fully IC configuration. This proves to be the lightest hexcopter configuration at the smallest feasible diameter. This weight statement includes oversized engines to allow for OEI safe flight with climb rates in excess of 900 ft/min (FAR 29.67 compatible).

Table 3: Airframe Weight Fractions

Item	Weight Fraction (%)	Material
Mufflers and Roll Cage	19%	Steel/Kevlar
Duct Shrouds	18%	CFRP/Titanium
Sub Structure	26%	CFRP
Rotor Mesh	3%	Steel
Skins	3%	CFRP
Fin and Seat	7%	Honeycomb/PEEK
Landing Gear	7%	Steel/Kevlar
Empennage Actuators	7%	~
Electronic Speed Controller	5%	~
Miscellaneous	4%	~

Table 4: Weights of the Vehicle

Component	Weight (lb_f)
Propulsion System	95.0
Power Distribution	20.0
Fuel	34.9
Airframe	74.2
Pilot	200.
MGTOW	424

4.1.2 DUCTED FAN CHARACTERISTICS

Each rotor is contained within a shroud equipped with a quasi-isentropic inlet. This design will ensure clean airflow into the rotors and increase the efficiency of the propulsion system by decreasing tip effects. Each duct is fabricated with a titanium ringed carbon shroud. Titanium rings provide the interface for the structural supports of the engines and stators. CFRP is used to both extend and shape the shroud and inlet and transfer loads to the rest of the airframe.

4.2 UNDERCARRIAGE AND MAJOR COMPONENTS LAYOUT

4.2.1 LANDING GEAR

The main gear of the Mamba is of a tripod configuration: two main gear in the fore and a single aft main gear. A series of outriggers located at the back of each main engine provide additional stability during loading operations. The front gear are integral to the roll cage and engine muffler assembly, and are comprised of an aramid epoxy composite surrounding an inner core of steel (used as the muffler). This arrangement ensures the operator is not at risk for burns in case of contact with the roll cage assembly. The main aft gear is an extension of the center keel beam of the substructure. The outer composite layer on the main gear is designed to handle all loads, and is sized based on the energy dissipation requirements during a hard landing.

Figure 12: Gear, Outrigger, and Seat Integration

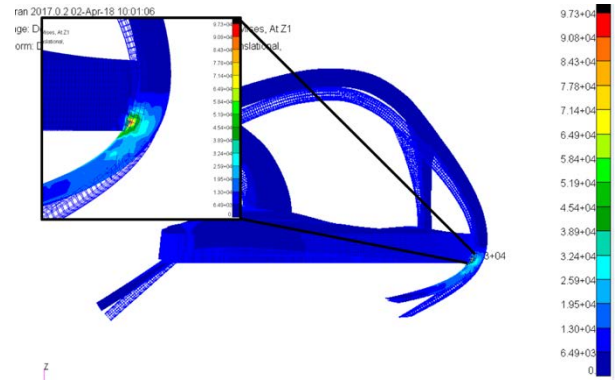

Figure 13: OEI Descent Landing Gear Analysis

The nominal OEI descent rate of 7 fps is used to size the gear for no failure, and a hard landing at 20 fps is used to size the total crush-out distance to ensure the pilot is decelerated at an equivalent rate less than 5g. From the nominal descent rate, to achieve pilot deceleration of 5g with a FS = 1.5 (3.33g), the required landing gear stroke (or total vertical deflection) is 0.23 ft (2.8 in). For the failure scenario at 20 fps, the total required failed crush-out distance is 1.87 ft.

From the FEM analysis, the vertical stroke of the landing gear under the nominal OEI descent rate is 3.2 in, and is sufficient for pilot load limitations without composite failure. At 20 fps, the gear/roll-structure is designed to fail and fold to dissipate energy, with total crush-out distance before operator impact exceeding the required 1.87 ft. Energy dissipation and structural frequency response may be determined from higher order methods or experimental work as part of the Phase II analysis risk reduction.

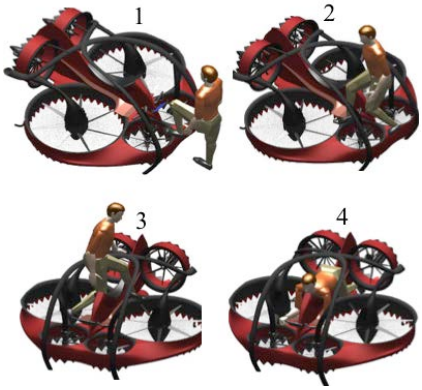

Figure 14: Operator Mounting

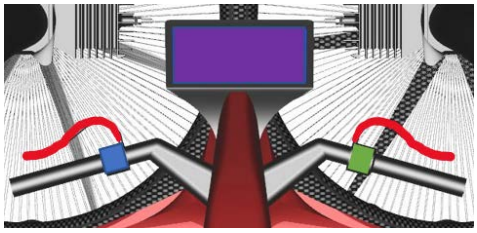

Figure 15: Pilot Control Layout

4.2.2 COCKPIT & USER OPERATIONS

The operator enters the vehicle from the front, depicted in Figure 15, wearing the flight suit (Figure 16). The flight suit is integral to the central seat with

multiple attachment points to ensure pilot safety during flight and a single point release to be used in emergency scenarios. The cockpit is designed to be familiar and approachable to any operator accustomed with motorcycle operations and is shown in Figure 14. The handlebars will act as the main flight control input system for the pilot. Altitude will be controlled via a thumbwheel on the left side of the handlebars, shown blue. Forward thrust is managed by another thumbwheel on the right side of the handlebars, shown green. The braking system will be controlled via a traditional brake lever on the handlebars, shown red. An iPad mini with ForeFlight, in conjunction with the Stratus 2S receiver, displays relevant real time flight information.

Ground operations include transport via flatbed to the flight area, and the placement of removable caster assemblies under each of the main gear for rolling across finished surfaces.

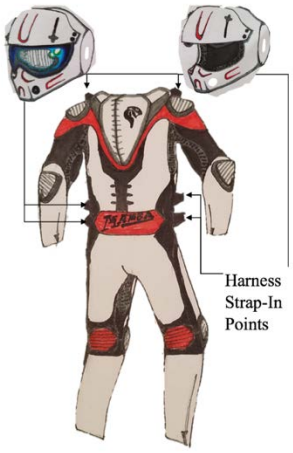

Figure 16: Flight Suit

4.3 STRUCTURAL LAYOUT

The main structural members of the vehicle include a central keel beam, stringers, and integral wire-splitters. The central keel beam distributes the loads of the vehicle longitudinally, and is a CFRP blade sized for maximum bending loads with a factor of safety of 1.5. The wire splitter bars will be sized in future risk reduction analysis for max speed impact with electric cable (simulating a full powered run through a power line.

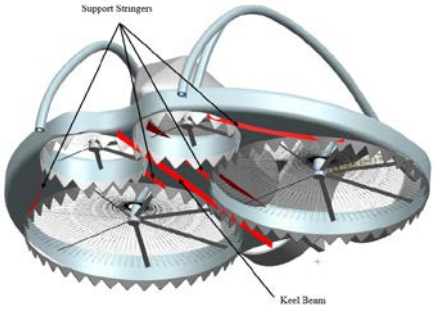

Figure 17: Keel Beam Layout with Supporting Stringers

4.3.1 INTEGRAL LANDING GEAR AND WIRE SPLITTERS

Preliminary sizing of the wire-splitters and roll cage assembly was achieved with finite element modeling (FEM) using the MSC Patran/Nastran solver suite. Static rollover (inverted) with the FS = 1.5 at MGWTO was used to determine the layup thickness of the outer aramid/epoxy composite, while the interior steel shell used as the integral muffler system is non-structural. This load case is further studied in 6.2. As anticipated, the results of the study show the critical region to be the change in curvature of the front gear. Stress levels within the composite indicate with 4 +/45 cloth lamina, the margin of safety in the composite exceeds 20% in any given ply and is critical in shear.

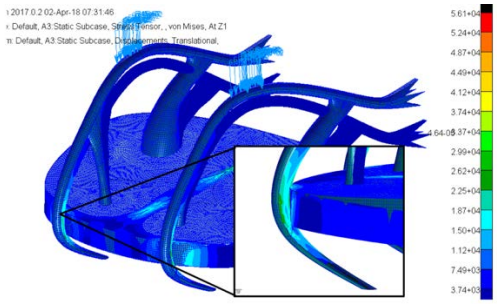

Figure 18: Static Roll Over Analysis

4.4 MAJOR SYSTEMS INTEGRATION

The fuel and battery systems layout is designed for triple redundancy and is shown in Figure 20. The avgas system, in blue, holds 3.77 gallons that service the main two engines. The 1.57-gallon fuel/oil mixture system, in red, provides fuel for the 4 auxiliary engines. Lastly the double redundant electric system, in green, provides electricity for the starters and avionics. The batteries used for this vehicle will be the 28Ah Prismatic Lithium-ion Battery Cell. All of the electrical/fuel lines will be fed through the spoke conduit system, illustrated in the MicroStator cross section in Figure 19. Two rotary actuators will be installed to provide the aft duct rotation. These actuators will be very similar to the FHA-C Rotary Actuator.

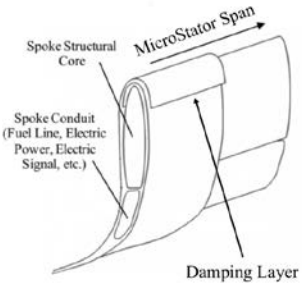

Figure 19: MicroStator Cross Section (US Patent Pending 62/659,026) Ref. (9)

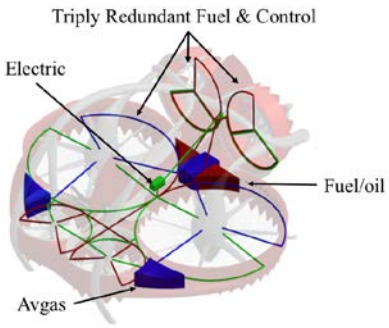

Figure 20: Mamba Primary Systems

5 FINAL CONFIGURATION

The final configuration of the Mamba is shown in Figure 21. The overall design has a maximum linear dimension of 95 inches and incorporates six lifting fans. The roll-cage structure is integral with the landing gear and engine muffling system, and serves as a means of cable deflection in case of power line impact. The pilot operates the vehicle from a semi-prone configuration, and has support options along the torso, legs, and forearms. Note, the MicroStator acoustic technology is shown, but the stators are of such a high aspect ratio that they become lost in the low resolution screen renders.

Table 5: Salient Characteristics

Parameter	Value	Units
Main Rotor Diameter	3.75	ft
Auxiliary Rotor Diameter	1.88	ft
Main Rotor Induced Velocity	55.1	ft/s
Auxiliary Rotor Induced Velocity	63.4	ft/s
Max Total Power at Altitude	105	hp
Number of Blades (all rotors)	7	(~)
Solidity (all rotors)	0.17	(~)
MGTOW	424	lb

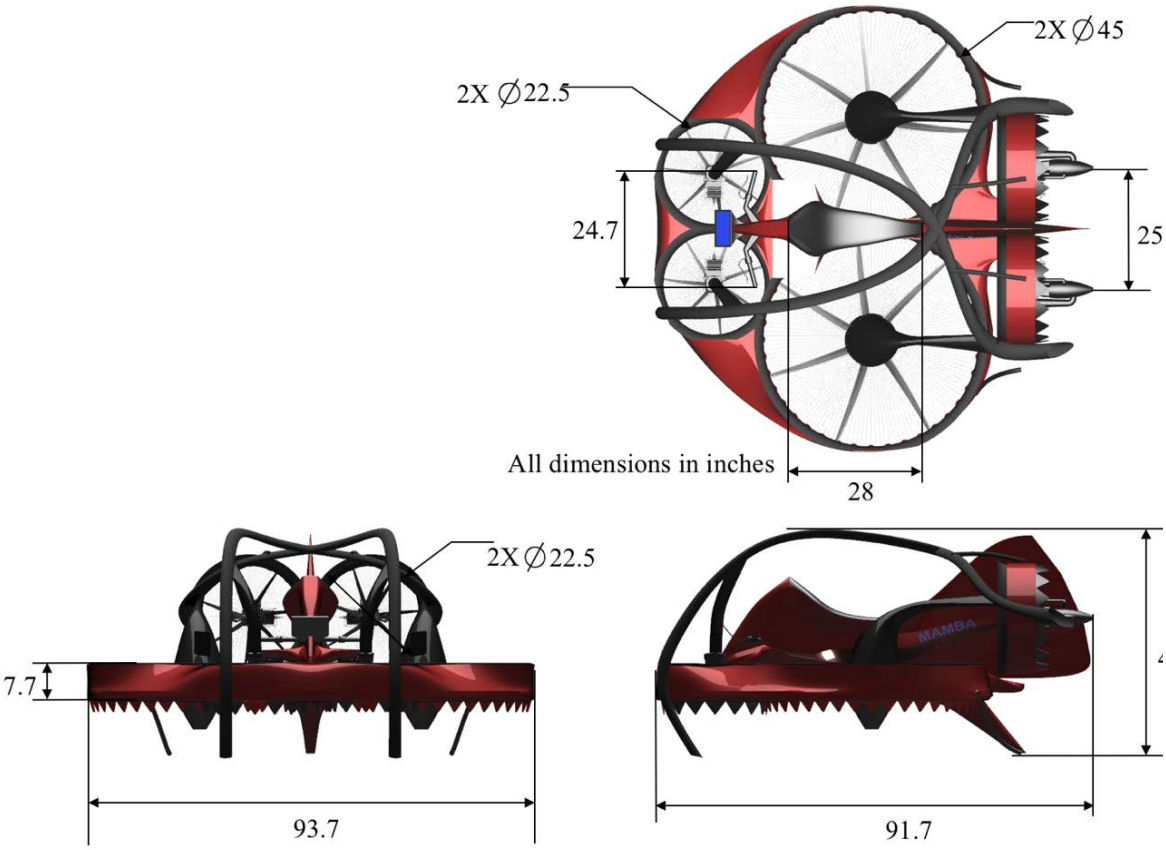

Figure 21: Mamba Final Configuration (SCALE 1:40)

6 SYSTEM INTEGRATION AND MODELING

6.1 ACOUSTIC CONSIDERATIONS

(Note: Patent Pending >3 dBA MicroStator Design Available for License (6)*)*

Patent pending MicroStator Acoustic Technology is used to reduce the rotor noise encountered in ducted fan configurations. This technology has the capability of reducing the overall SPL by greater than 3dBA when juxtaposed with conventional rotor/stator configurations. These stators are pretensioned high aspect ratio members used to transfer the loads of the propulsor to the duct, serve as a structural mesh to prevent operator or bystander contact with the rotors, and as a means of shifting the sound field energy to higher frequencies when compared with low aspect ratio stators. The MicroStators are used in conjunction with other conventional rotor and engine noise suppression techniques to ensure the Mamba achieves marketable SPL during operation.

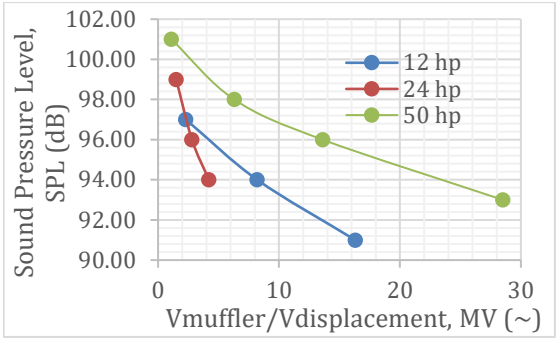

Figure 22: 2-Stroke Engine SPL Trends with Muffling Volume at 5 ft Ref. (11)

Another means of rotor SPL suppression is achieved with passive damping layers within the shrouds: these are comprised of a narrow layer of aramid honeycomb composite sandwiched between perforated carbon face sheets. This layer acts as a series of Helmholtz resonators that may be tuned to damp high narrowband SPL regions (such as rotor-stator interaction tones).

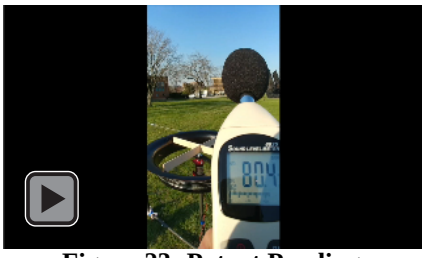

Figure 23: Patent Pending MicroStator Technology Demonstration

Engine noise, one of the largest components of overall SPL, is damped with large mufflers integrated into the wire splitters and roll bars. As SPL reduction scales with muffling volume, exhaust is routed throughout the length of these roll bars before exiting behind the vehicle.

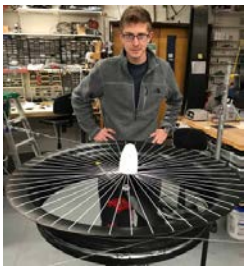

Figure 24: MicroStator Technology (US Patent Pending 62/659,026)

Jet noise caused by the shearing action between the rotor exit flow and ambient air is also mitigated using standard techniques. Chevrons are designed around each of the duct nozzles to induce vortices that enhance flow mixing. This mixing will reduce the cohesive eddy structures in the exhaust that are the primary source of jet noise.

During takeoff and landing at full power, noise will be increased due to ground reflection. This noise may be mitigated by applying acoustic foam to the underneath side of the main airframe. As noise is reflected from solid surfaces, reflections that intersect the vehicle may be absorbed in this foam layer. The foam will adversely affect the drag characteristics of the airframe in forward flight, but noise was deemed critical by the authors. Preliminary noise estimates for the full vehicle may be compiled from individual sources with existing trends (Figure 22) using the methodology in NASA TR 32-1462 (7), conservatively assuming constructive noise alone. The same reference may also be used to estimate the SPL at a distance R from the source. The estimated SPL for the vehicle at MGTOW in hover at altitude is 95dBA for an operator without hearing protection, and 66.7dBA at 50 ft.

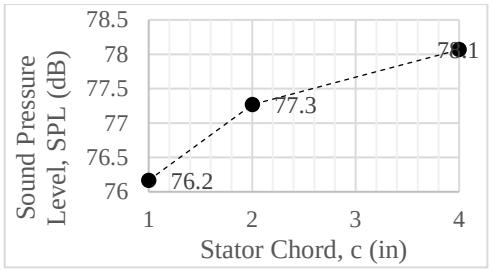

Figure 25: SPL Scaling with Stator Chord

6.1.1 Rotor Integration Acoustic Trends

Acoustic testing performed as a portion of the University of Kansas AE 748 Helicopter Aerodynamics course was used to project the sound power level of different rotor/stator lifting fan configurations. The first trend documented was sound as a function of distance, and the results follows the theoretical inverse square law, as anticipated. The next trend found was in relation to stator chord size, which was tested 6.5" from the top of the rotor (Figure 25). Lastly the trend of sound and distance from the stator to the propeller was found (Figure 26). As shown, the relationship is relatively linear with the sound decreasing as the distance from the rotor increases.

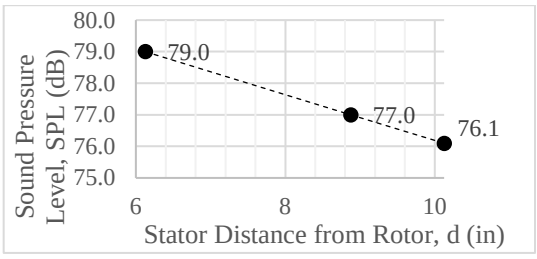

Figure 26: SPL Scaling with Rotor Clearance

6.2 PROPULSION INTEGRATION & MODELING

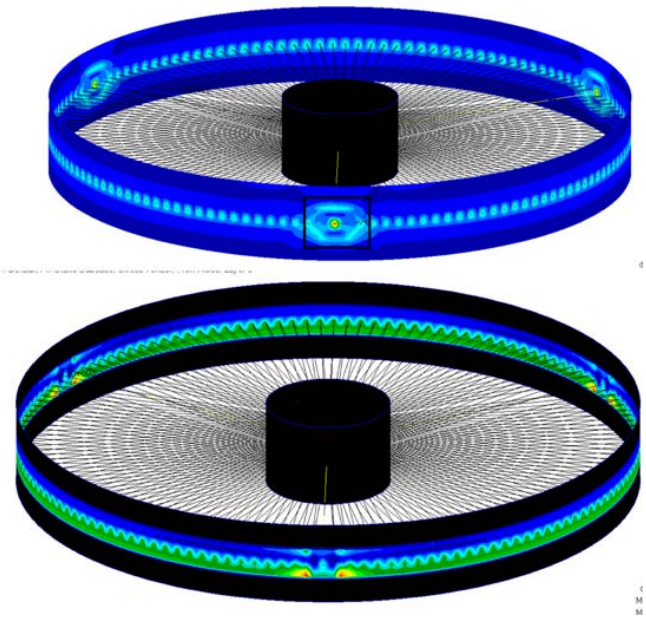

Figure 27: Main Duct Critical Stress Concentrations

The transfer of loads to the main structure through the MicroStator Acoustic Technology was studied with a Patran/Nastran FEM. A titanium ring (.032" thickness) is used to transfer the predominately tensile stresses in the MicroStators to the carbon duct. The duct itself is comprised of four layers of +-45 cloth CFRP. Three hollow stator sections (used to carry fuel to the engine) are modeled below the main MicroStator mesh. Figure 26 shows the critical stress distributions in the carbon duct and titanium support ring. Each of the 142 MicroStator pairs is modeled as a elliptic section (representing an aerodynamic shape) with a duct planar thickness of 0.058" prestressed to 100 psi. Under the critical load case (max thrust with FS = 1.5), the composite is critical in compression at the surface layer with a normal stress margin of 1.29. The titanium ring is also critical in compression and has a margin of greater than 4 at the most critical element (at thickness transitions to the remaining structure). The authors note the increased number of stators in this configuration limits the ovality modes of the duct to higher harmonics that experience increased atmospheric attenuation in noise transmission.

6.3 ROTOR DESIGN

The propulsion system is comprised of two systems: rotors 1 and 2 are designed for primary lift, and rotors 3, 4, 5, and 6 are designed for aircraft stability and control. Each rotors is shrouded with a quasi-isentropic duct as discussed in Section 4.1.2. to ensure increased power efficiency and support noise mitigation. In addition, the shrouds provide hardpoints for the MicroStator mounting (not shown in Figure 28 for clarity).

The rotors for each duct are designed using blade element momentum theory (BEMT) to improve performance. BEMT approximates the rotors as a series of airfoil blade sections and uses incompressible momentum theory for determining inflow, lift, and drag characteristics along the span of the individual rotors blades. Blade performance can be estimated for

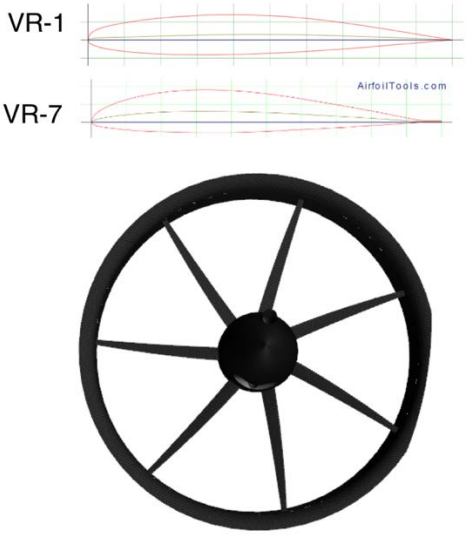

Figure 28: Main Rotor & Stator Design

properties such as reference pitch, twist, and taper ratio. Rotors 1 and 2 are designed for the hover condition to minimize the power consumption. The remainder are designed for control authority in one engine out scenarios.

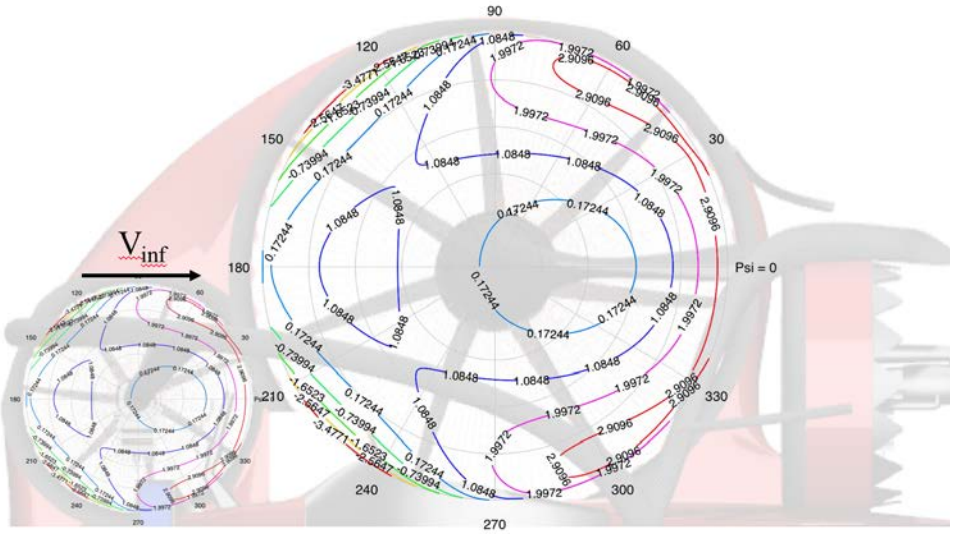

Figure 29: Induced Velocity Field for Rotors 2 and 4 V_i/V_{i0} at 60 kts

The resulting main rotor is a 7 bladed propeller with a disk solidity of 0.17. Each blade is linearly tapered with a tip chord to root chord ratio of 1:2.75, and has a blade twist of -10 degrees blade root to tip. The airfoil sections are members of the Boeing VR airfoil series. This family of airfoils was chosen for its proven use in other rotorcraft and for the consistency in general cross-sectional airfoil shapes from root (reducing manufacturing costs). The induced velocity field across the rotor is then solved using perturbation theory with the Mangler and Squire as noted in Reference (8). The normalized induced velocity field across the main rotor at V_{max} is shown in Figure 29.

7 CENTER OF GRAVITY ANALYSIS

For the weight and balance of the Mamba, two operations were analyzed: on ground operations, and in flight operations. It is noted that operator position is the differentiator between these two conditions.

CG excursions for these two operations can be seen in Figure 30. The lower horizontal axis shows the CG location while the top axis shows the location as percent of the main engines location. The largest CG excursion for in flight operations is 1.5 at 4% main engine location. The largest CG excursion for on ground operations is 7.7 at 17%. The on-ground excursion is compensated with the outriggers installed to prevent tip over.

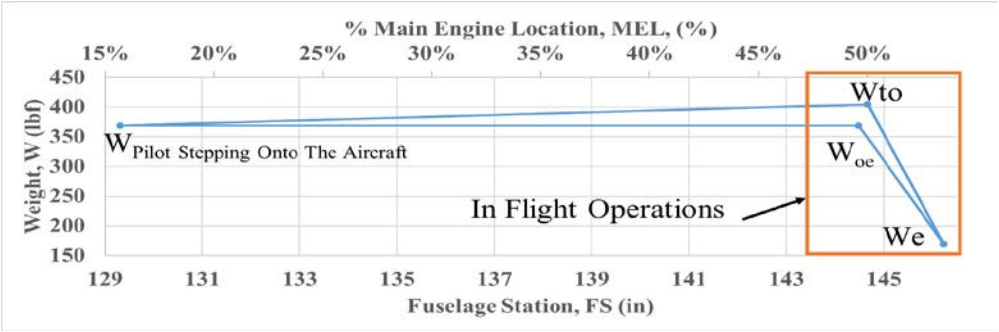

Figure 30: CG Excursion Diagram

8 PERFORMANCE ANALYSIS

8.1 POWER REQUIRED

The performance of the Mamba may be characterized in both hover and forward flight using the methods outlined in Reference (5). In OGE hover, a 25% thrust margin was designed to ensure gust rejection, and this represents the maximum expected power consumption by the propulsion system (9). In forward flight, Equation 2 may be obtained by applying the conservation of momentum along a vector perpendicular to the disks. The total power required may then be determined as a sum of the parasite, induced, and profile power required in forward flight (5). The results of the power required analysis at MSL are shown in Figure 31. Note, the speed for maximum endurance occurs near 60 kts and is altitude dependent. The rotor tip speed is prescribed as M = 0.61. With these analysis techniques, the disk loading required from each of the main lifting fans may be tabulated in the hover condition ($DL_{1,2}$ = 13.5 lb/ft^2, $DL_{3\text{-}6}$ = 25.5 lb/ft^2).

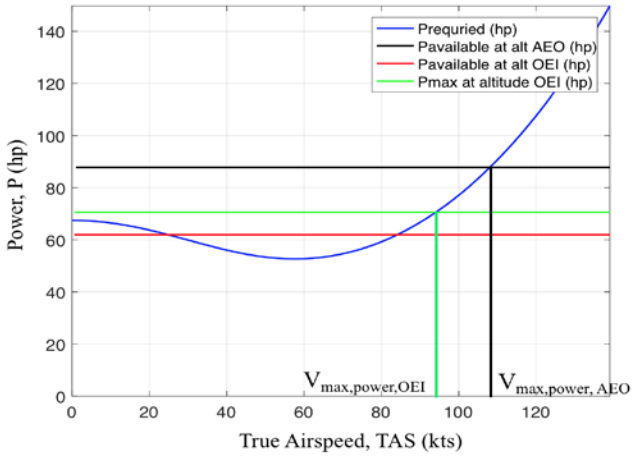

Figure 31: Power Required & Available at 5,000 ft MSL

8.2 CLIMB-OUT AND ROTOR EFFICIENCY

In an OEI scenario, the remaining engines are run at max rated power to achieve climb-out and controlled descent. The OEI climb rate is given in Figure 32. The figure of merit (FM) of the system may also be defined. With a known thrust coefficient and blade parameters described in 6.3, the FM is written:

$$FM = 1/(\kappa + \frac{\frac{\sqrt{2\rho}}{T}P_0}{\sqrt{DL}}) \qquad \text{[Ref. (5)]} \qquad \text{(Eq. 3)}$$

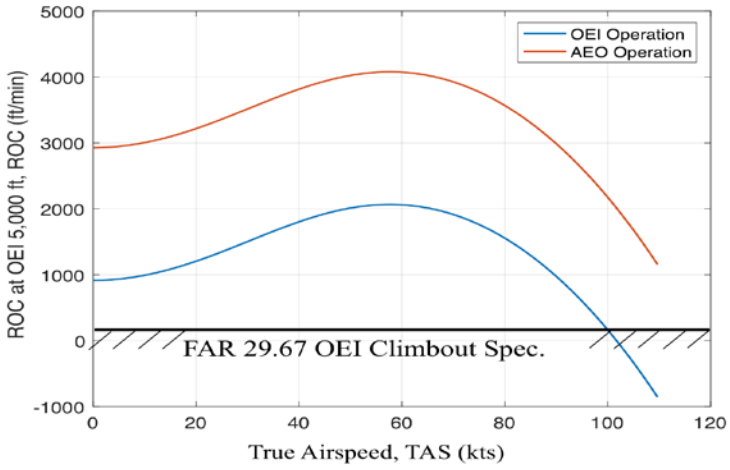

Figure 32: Climb-Out Capability at 5,000 MSL

These values are numerically solved for as a function of inflow ratio. The main rotor experiences a BEMT calculated figure of merit of 0.75 in hover, while the auxiliary rotors operate at 0.82. Excess power in a given flight state may be used to accelerate the vehicle in maneuver or climb. The results of the climb-out capability during critical OEI operation assuming max engine power is given in Figure 32.

9 STABILITY & CONTROL ANALYSIS

The kinematic equations for general aircraft (Eq. 4) and the control forces and moments generated for this hexcopter were estimated in Eq. 5. These equations can be combined into a generalized linear state space model using linear perturbation theory. Under the assumption of constant rotor power output, the perturbed rotor thrust can be related to perturbed inflow by the negative nominal thrust over nominal inflow. The torque generated by the motors may be found using the rotor averaged lift to drag ratios and the mean drag radius from the BEMT analysis. Thus the perturbed induced velocities–and the rotor forces and moments—can be associated with perturbations of vehicle translational and rotational velocities.

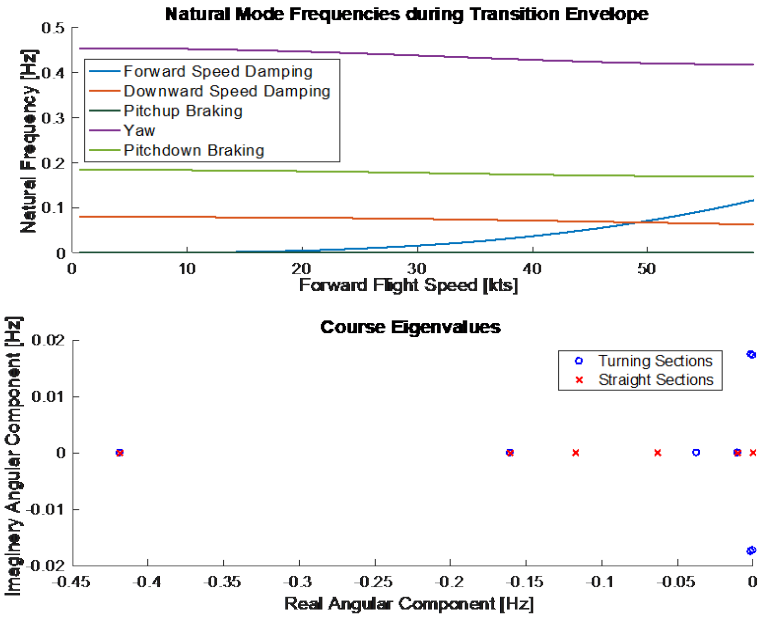

Figure 33: Mamba Stability in Transition and Dash

$$\begin{pmatrix}\dot{U}\\ \dot{V}\\ \dot{W}\end{pmatrix} = \begin{pmatrix}RV - QW\\ PW - RU\\ QU - PV\end{pmatrix} + \frac{1}{M}\begin{pmatrix}F_X\\ F_Y\\ F_Z\end{pmatrix}\begin{pmatrix}\dot{\phi}\\ \dot{\theta}\\ \dot{\psi}\end{pmatrix} = \begin{pmatrix}1 & sin(\phi)tan(\theta) & cos(\phi)tan(\theta)\\ 0 & cos(\phi) & -sin(\phi)\\ 0 & \frac{sin(\phi)}{cos(\theta)} & \frac{cos(\phi)}{cos(\theta)}\end{pmatrix}\begin{pmatrix}P\\ Q\\ R\end{pmatrix}\begin{pmatrix}\dot{P}\\ \dot{Q}\\ \dot{R}\end{pmatrix}$$

$$= J^{-1}\left(\begin{pmatrix}0 & R & -Q\\ -R & 0 & P\\ Q & -P & 0\end{pmatrix} J \begin{pmatrix}P\\ Q\\ R\end{pmatrix} + \begin{pmatrix}L\\ M\\ N\end{pmatrix}\right) \qquad \text{[Ref. (10)]} \qquad \text{(Eq. 4)}$$

$$\begin{pmatrix}F_X\\ F_Y\\ F_Z\\ L\\ M\\ N\end{pmatrix} = \begin{pmatrix}0 & 0 & 0 & 0 & 0 & 0\\ 0 & 0 & 0 & 0 & 0 & 0\\ -1 & -1 & -1 & -1 & -1 & -1\\ -Y_{1,2} & Y_{1,2} & -Y_{3,4} & Y_{3,4} & -Y_{5,6} & Y_{5,6}\\ X_{1,2} & X_{1,2} & X_{3,4} & X_{3,4} & -X_{5,6} & -X_{5,6}\\ -\bar{r}_{D,1,2}\left(\frac{\bar{D}}{\bar{L}}\right)_{1,2} & \bar{r}_{D,1,2}\left(\frac{\bar{D}}{\bar{L}}\right)_{1,2} & -\bar{r}_{D,3,4}\left(\frac{\bar{D}}{\bar{L}}\right)_{3,4} & \bar{r}_{D,3,4}\left(\frac{\bar{D}}{\bar{L}}\right)_{3,4} & -\bar{r}_{D,5,6}\left(\frac{\bar{D}}{\bar{L}}\right)_{5,6} & \bar{r}_{D,5,6}\left(\frac{\bar{D}}{\bar{L}}\right)_{5,6}\end{pmatrix}\begin{pmatrix}T_1\\ T_2\\ T_3\\ T_4\\ T_5\\ T_6\end{pmatrix} \qquad \text{(Eq. 5)}$$

$$\delta\vec{v_i} = -\delta w + \delta\omega \times \vec{r}_{motors} \qquad \text{(Eq. 6)}$$

Numeric inflow calculations at thrusts required for varied forward flight speeds will yield the state A matrix and, by extension, the inherent dynamics stabilities and changes in frequency of the

natural dynamic modes during the transition envelope. The Mamba was found to be stable during transition to forward flight.

The Mamba was analyzed for fly-off dash at a constant ground speed of 100 feet per second at a 10 degree forward deck tilt and 20 degree bank angle turns. The eigenvalue frequencies are shown in Figure 33. Both the straight sections and turning sections of the course exhibit low frequencies and the turning sections have two under damped oscillatory modes. However, all modes are stable.

In forward flight, an analysis of the aircraft pitch stability for various flight speeds with respect to the tilt angle of the aft engines was completed (Figure 34) The Mamba is forward flight limited to a maximum forward flight velocity of 120 ft/s with a deck angle of -10 deg. due to engine sizing and placement.

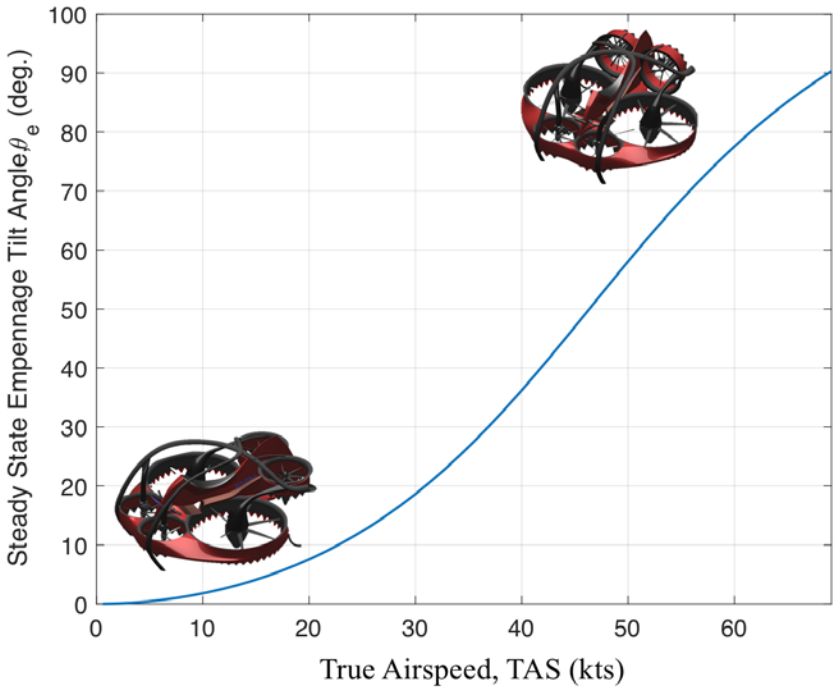

Figure 34: Required Empennage Tilt Angle

10 MANUFACTURING CONSIDERATIONS

10.1 FACILITIES

The composites laboratory of the University of Kansas will be used to produce the primary structure of the Mamba. Components with additional complexity such as the engine exhaust assembly are outsourced as noted in Table 6. Final assembly will take place in house at the University of Kansas.

- KU Composites Laboratory: Manufacturing and Assembly
- KU Mal Harned Propulsion Laboratory: engine testing
- KU Structural Dynamics & Acoustics Laboratory: structural testing and modal characterization
- CReSIS Anechoic Chamber: acoustic testing (subscale model)
- Clinton International Model Airport: subscale flight testing
- Smoky Hill Gunnery Range, Fort Riley Test Range, and Sunflower Army Ammunition Plant: full scale range and endurance testing

Table 6: Manufacturing Procedural Breakdown

Duct Structure (forward and main ducts, skins, keel beam, auxiliary stringers) – hand layup and oven cured, {Solvay, Krayden}. Titanium ring structure formed in house.	Batteries - Supplied by an outside source.
Aft Duct Rotation Mechanism – purchased {Rockwell Collins/ Moog Inc.}	Rotors – {KU Composites Laboratory or other}
Chevrons – neoprene shaped in house	Exhaust Manifold (plasma spray or electroplated) – {ASB Industries Inc., A&A Coatings Inc.}
Seat Structure – aramid/epoxy hand layup in house	MicroStators – {McMaster-Carr/Airparts Inc.}
Seat Finishing – purchased externally	Roll Cage /Wire Splitters – Hand woven sleeve {KU Composites Laboratory}
Controls – {Honeywell}	Anechoic Foam – {General Plastics}
Flight Computer – {Garmin/Honeywell}	Engine Assemblies – {Rotapower/3W}

10.2 ASSEMBLY PROCESS

The major composite assemblies (ducts, skins, keel structure, stringers, seat) are produced at KU using hand layup. These components are then co-cured offsite with the deck skins. The seat is then attached to the primary substructure and the fuel tanks mounted. Fuel tanks are fixed beneath the deck skins and sealed. Engine assemblies are then trued to the center of each duct using the MicroStator suspension system. After routing the fuel and electric lines beneath the main deck skins, acoustic foam is applied to the entire base of the structure. The completed roll cage/wire splitter assembly is then mounted to the main frame and the rear ducted propulsors suspended. Chevrons are then installed around the base of each duct, and the completed aircraft is painted.

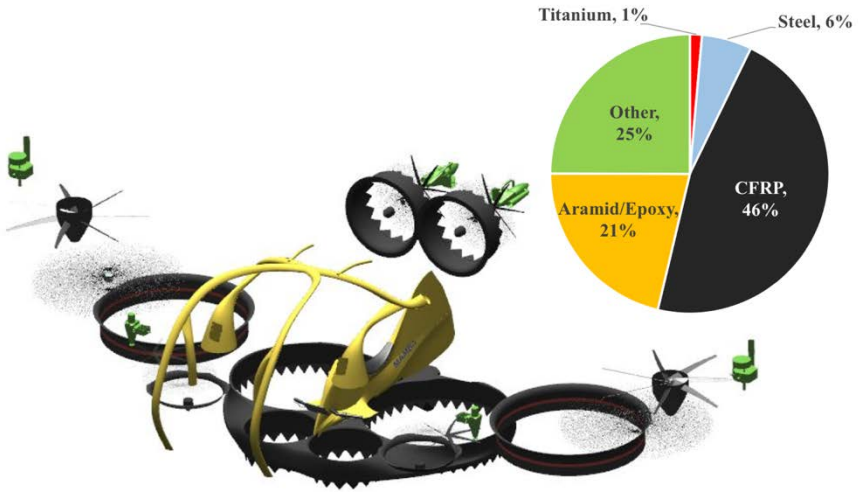

Figure 35: Materials Breakdown

11 TECHNOLOGY READINESS AND RISK SUMMARY

As the Mamba concept will undergo initial build in the fall of 2018, only technology, materials, and manufacturing procedures that meet TRL 6 were implemented on this vehicle. Flight critical systems were developed only from TRL9 and above technologies. Key enabling technologies and their relative associated risk are displayed in Table 7.

Table 7: Technology Risk Summary

	Consequence of Risk Occurrence				
Probability	Very Low	Low	Moderate	High	Very High
Very Low		Conventional Acoustic Suppression	Materials/Manufacturing	Propulsion Sys. Availability	
Low			Shrouded Fan Performance	Certification	
Moderate		Patent Pending MicroStator Concept			
High		Urban Scalability			
Very High					

The acoustic suppression techniques and potential for additional power generation outlined in in the patent pending MicroStator Acoustic Suppression is a key enabling technology in the noise portion of the GoFly design requirements, but is not flight critical. Conventional acoustic suppression methods detailed in Section 6.1 are well understood and implemented in the aerospace industry. The Rotapower 300cc engines, are not in full production at this time of this design. The engines have been manufactured for testing and evaluation, and are thus deemed to be the most critical technology risks for the concept at TRL 6. Conventional materials and manufacturing techniques are detailed in 10. Risk mitigation for the lifting fan performance will be achieved in the flight testing phase of the program scheduled for fall 2018. Certification of the Mamba would take place under FAR 21 as previously discussed . As it is a shrouded rotor concept, the risk of not certifying in the US is greatly reduced. Urban scalability is at the highest risk (6) for failure, but as this iteration of the concept is intended to be used as a recreational personal use vehicle, this risk is not crucial to the overall concept at this phase.

12 REFERENCES

1. **Anon.** Avro Canada VZ-9 Avrocar. [Online] https://en.wikipedia.org/wiki/Avro_Canada_VZ-9_Avrocar.
2. Anon. Hiller VZ-1 Pawnee. [Online] https://en.wikipedia.org/wiki/Hiller_VZ-1_Pawnee.
3. Anon. Glenn L. Martin. [Online] https://en.wikipedia.org/wiki/Glenn_L._Martin.
4. **Moller International.** Moller International. *Moller International.* [Online] https://moller.com/.
5. **Leishman, J. G.** *Principles of Helicopter Aerodynamics.* s.l. : Cambridge Univeristy, 2002.
6. **Barrett, R. M., et al.** *Acoustic Noise Suppressing Ducted Fan Propulsor Mounting Arrangement and Treatments. 62/659,026* 2018. Provisional Pending.
7. **Marte, J. E., Kurtz, D. W.** *A Review of Aerodynamic Noise From Propellers, Rotors, and Lift Fans.* Pasadena, CA : National Aeronautics and Space Administration Jet Propulsion Laboratory, 1970. TR 32-1462.
8. **Bramwell, A. R. S, Done, G., Balmford, D.** *Bramwell's Helicopter Dynamics.* Delhi : Replika Press, 2001. ISBN 0-7506-5075-3.
9. **Lee, G. L.** *Muffling Volume Acoustic Trends on 2-Stroke Engines.* s.l. : MASs LLC.
10. **Beard, R. W., McLain, T. W.** *Small Unmanned Aircraft: Theory and Practice.* Princeton : Princeton Univeristy Press, 2012. ISGN 978-0-691-14921-9.
11. **Anon.** GoFly. *Hero X.* [Online] 2017. https://www.herox.com/GoFly.